PHILOSOPHICAL TRANSACTIONS OF THE ROYAL SOCIETY A MATHEMATICAL, PHYSICAL & ENGINEERING SCIENCES

Ultrasonic Measurement of Internal Temperature Distribution [and Discussion]

H. N. G. Wadley, S. J. Norton, F. Mauer, B. Droney, E. A. Ash and C. M. Sayers

Phil. Trans. R. Soc. Lond. A 1986 **320**, 341-361
doi: 10.1098/rsta.1986.0123

Phil. Trans. R. Soc. Lond. A **320**, 341–361 (1986)
Printed in Great Britain

Ultrasonic measurement of internal temperature distribution

H. N. G. Wadley,[1] S. J. Norton,[1] F. Mauer[1] and B. Droney[2]

[1] *National Bureau of Standards, Gaithersburg, Maryland* 20899, *U.S.A.*

[2] *Bethlehem Steel Corporation, Bethlehem, Pennsylvania* 18016, *U.S.A.*

Implementation of advanced materials processing strategies are presently hampered by a lack of adequate process-control sensors. For the processing of basic materials, such as steel and aluminium, an internal temperature-distribution sensor is needed. For these metals, the velocity of ultrasound is well known to be a strong function of temperature. We have therefore explored the feasibility of precisely measuring the velocity–temperature relation for a particular steel grade and using this to convert an ultrasonic-velocity distribution (tomogram) for a hot steel body to an internal temperature distribution. To overcome the usual need in conventional tomography for many thousands of path-integral measurements along intersecting ray paths, *a priori* heat-flow information has been incorporated into the reconstruction algorithms. As a result, for uniformly cooling bodies with the simple geometries usually encountered (e.g. circular, square or rectangular cross sections), the number of measurements can be reduced from many thousands to as few as three to five. Initial experiments on austenitic steel samples of cylindrical and square cross section by using non-contact ultrasonic techniques have shown that this approach yields acceptable temperature profiles at temperatures of up to 750 °C.

1. Introduction

The processing of materials from the most basic, such as the casting of steel, to the most advanced, such as the epitaxial growth of optical or electronic materials, is undergoing a radical change. Recent scientific advances have greatly improved the understanding of many of the phenomena involved in processing. This, in turn, has resulted in the emergence of sophisticated process models capable of predicting the effect of process variables upon, and the microstructure properties of, processed material. These process models are now becoming the heart of automated control systems for materials processing. These systems promise both productivity and quality enhancements for existing processes and the more reliable processing of many advanced materials that hitherto were considered too unstable for commercial development (Mehrabian & Wadley 1985).

As we look toward the future, it is anticipated that automated control of materials processing will consist of three interlinking systems. *Sensors* will continuously measure, in-process, critical microstructure and process variables without perturbation to the process. Sensor data will then be utilized by *predictive models* to evaluate the current state of processing and, with the aid of expert systems and other artificial intelligence techniques, a new, optimum set of process conditions will be determined. Finally, *control* systems will stably implement these conditions.

While major strides have been made in both predictive process modelling and process control, the development of materials-processing sensors has lagged behind and is the limiting factor for many potential applications of automated process control. The required sensors for materials processing are quite unlike those of other industries. For example, a list of sensor needs

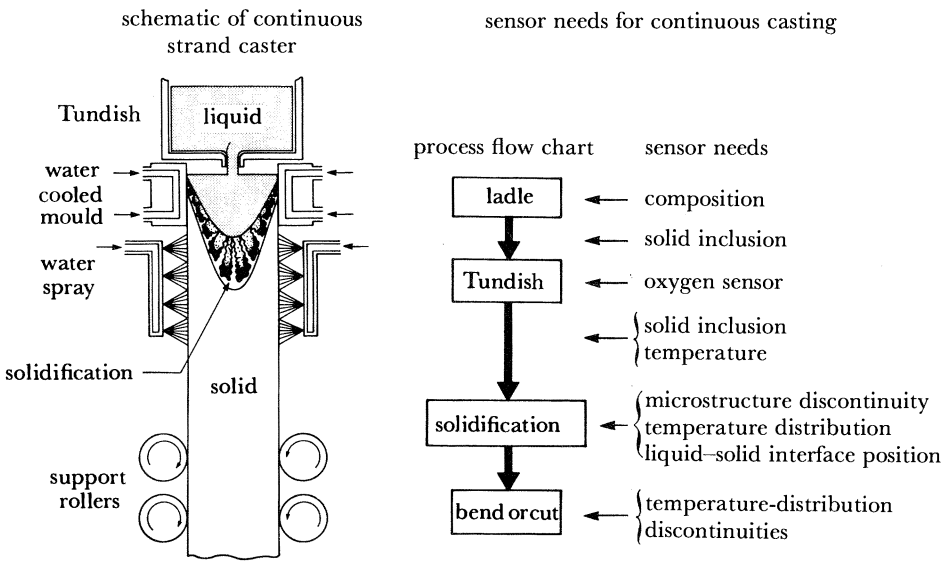

FIGURE 1. Schematic diagram of a metal continuous caster and the sensor needs for the casting of steel.

for the continuous casting of metals (figure 1) would include the measurement of the concentration of dispersed inclusions and the continuous chemical composition in the liquid-metal internal-temperature distribution during solidification, and detection of discontinuities (porosity, segregates, cracks) after solidification.

Because it is essential that these sensors neither perturb the material they interrogate nor disrupt the process they monitor, they can truly be considered new applications for non-destructive evaluation (NDE). In fact, the candidate approaches to some of these measurement needs are based upon traditional NDE techniques, such as ultrasonics and eddy currents.

The study reported here is concerned with the development of a sensor for measuring internal temperature distributions in solid or solidifying metal bodies. To date, it has focused upon steel, but the principles apply to the processing of other materials of both metallic and non-metallic character. This research is a collaborative effort between the American Iron and Steel Institute (AISI) and the National Bureau of Standards (NBS), a laboratory of the U.S. Department of Commerce. The AISI recognized the central importance of sensors for materials processing at least as early as 1979. In 1982, a NBS–AISI workshop at NBS identified the urgent need for four steel sensors, one of which was the measurement of internal temperature distribution (Mehrabian *et al.* 1982). This sensor was envisaged to have applications during continuous casting and during slab reheating, provided that the sensors could non-invasively measure temperature to within ± 10 K with 10 mm spatial resolution. It is toward this goal that we have been working.

Usually temperature is not directly measured; rather one relies upon the measurement of temperature-dependent physical properties that have been previously calibrated against temperature. Numerous temperature-dependent physical properties are today accessible to measurement. For sensor purposes, however, the most promising will be those amenable to a non-contact measurement with the potential to probe the sample interior (through, say, several centimetres of steel). Measurements of thermal radiation (optical pyrometry) or lattice parameter (X-ray diffraction), although non-contact, unfortunately only provide surface or near-surface temperature measurements. Two more promising approaches are the

use of eddy-current techniques to measure subsurface electrical resistivity, and ultrasonic-velocity techniques for the measurement of elastic modulus:density ratio.

The electrical resistivity of all metals is well known to be a reasonably strong function of temperature with typical changes of the order of *ca.* 0.2% per kelvin for pure α-iron (BCC phase). Coils encircling the sample provide a convenient method for inducing eddy currents and thus for measuring resistivity in a non-contact manner. The variation of the frequency (and hence the depth of penetration) provides a basis for systematically probing through the depth of a conducting sample. The inverse techniques used to reconstruct an electrical resistivity (and hence temperature) profile from such measurements are, however, only now emerging and, at present, lack the precision (2–5%) required for accurate temperature measurements (Kahn *et al.* 1986). Moreover, it is experimentally difficult to perform measurements at low enough frequency (e.g. a few hertz) to significantly penetrate thick (*ca.* 20–30 cm) steel.

The velocity of ultrasound has for a long time been known to be strongly influenced by temperature in most materials. In steels, changes of 0.5–1.0 $\mathrm{ms^{-1}}$ per kelvin are typical for longitudinal waves (Kurz & Lux 1969). A change of 1 K in the average temperature of a block of steel at 750 °C corresponds to a velocity change of 2 parts in 10^4. In the laboratory, time-of-flight techniques for measuring the velocity of ultrasound are routinely capable of this order of precision. In addition, the recent development of pulsed-laser ultrasonic generation and non-contact electromagnetic acoustic transducers (EMATS) promise a non-contact, and thus non-invasive, measurement methodology. These considerations have led us to begin the development of an ultrasonic temperature distribution sensor.

We describe below recent progress in three key areas associated with an ultrasonic sensor: (1) development of reconstruction methods (including the incorporation of *a priori* information) for the determination of a velocity (and hence temperature) profile within a sample; (2) development of accurate methods for obtaining standard reference data that relate ultrasonic velocity to temperature for a variety of specific grades of steel and (3) the design and evaluation of experimental, non-contact methods for ultrasonic generation and measurement in hot steel bodies. Although the metal of interest in our current work is steel, the application of this research to other metals, such as aluminium, is anticipated to introduce few new difficulties.

2. Reconstruction theory

(*a*) *Circular symmetry reconstructions*

Consider the problem of reconstructing a circular cross-sectional map of the temperature through a solid cylinder. If heat diffuses uniformly through the surface, the temperature will rapidly approach a radially symmetric distribution. In this state, the unknown temperature field is defined by a one-dimensional function of radius, $T(r)$. Our objective is to use ultrasonic time-of-flight (TOF) measurements to reconstruct the radial velocity profile, $v(r)$, from which we then compute the temperature profile, $T(r)$.

A convenient scheme for rapidly generating multiple TOF measurements consists of transmitting from a single ultrasonic source at one point on the cylinder, and receiving with an array of detectors spaced around the circumference (figure 2). This is known as a 'fan-beam' measurement in the terminology of medical X-ray tomography. Let τ_m denote the measured TOF over a path of length L_m. Then,

$$\tau_m = \int_{L_m} \frac{\mathrm{d}l}{v(r)} \quad m = 1, 2, \ldots, M, \tag{1}$$

where M is the number of paths. In practice, M is small because of the limited time available for measurement, as well as the cost and complexity associated with attempting numerous simultaneous measurements.

Several techniques exist for the tomographic reconstruction of velocity, and hence temperature, from the path-integral measurements τ. When the number of unknowns is small, which is the case here because M is necessarily small, a direct inversion can be attempted by subdividing the cylindrical cross section into equally spaced, radially symmetric pixels or annular regions of assumed constant temperature (figure 2). Given a sufficient number of TOF measurements over paths intersecting these annuli, the temperature may be computed in each annulus by inverting a linear system of algebraic equations. If more measurements than unknowns (number of annuli) are obtained, the mean pixel temperatures can be estimated in a least-squares fashion.

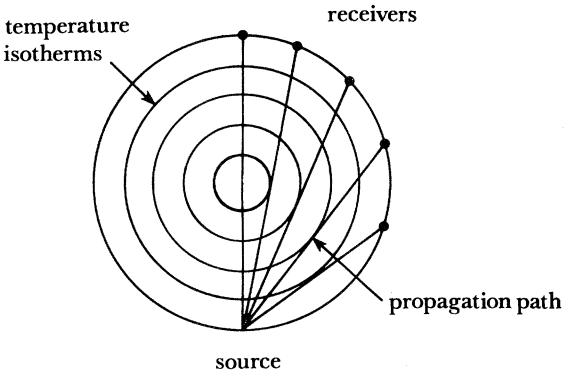

FIGURE 2. A 'fan beam' ray pattern for ultrasonically sampling the temperature profile of a cylinder.

The above approach was applied to TOF data measured in our initial experiments (Norton *et al.* 1984). Unfortunately, ill-conditioning of the resulting system of equations, even for the over-determined case, gives rise to a large amplification of measurement errors. Less sensitivity to measurement uncertainty can be achieved by 'regularizing' the inverse problem. Many such regularizing schemes exist; examples include imposing an *a priori* smoothing constraint on the solution, reconstructing under a maximum entropy constraint, or eliminating small singular values from the matrix to be inverted. In general, the incorporation of *a priori* constraints of any kind helps mitigate reconstruction ill conditioning.

We have exploited a different kind of 'regularization' of the reconstruction problem by noting that temperature cannot be an arbitrary function of space and time, but must obey the heat-conduction equation subject to certain boundary conditions. The boundary conditions are, in turn, determined by the geometry of the body and the rate at which heat is flowing across its boundaries. As a result, our approach has been to express the unknown temperature distribution as an expansion in the eigenfunctions of the heat-conduction equation. The coefficients in the expansion determine the reconstructed temperature and represent the 'unknowns' to be computed from the TOF measurements. In the reconstruction, spatial resolution is determined by the number of terms retained in the expansion. As a general rule, however, the numerical ill-conditioning of the inversion problem increases rapidly with the number of terms retained (i.e. number of unknowns). Thus, in general, an inherent trade off exists between ill conditioning (or error sensitivity) and resolution.

Below, we illustrate this approach for the case of a cylinder with radially symmetric heat flow. Under these conditions, the temperature obeys the heat-conduction equation

$$\frac{1}{r}\frac{\partial}{\partial r}\left(r\frac{\partial T}{\partial r}\right)=\frac{1}{\kappa}\frac{\partial T}{\partial r}, \tag{2}$$

where κ is thermal diffusivity, subject to the radiation boundary condition

$$\partial T/\partial r+h(T-T_{\mathrm{amb}})|_{r=R}=0. \tag{3}$$

In (3), $h=H/K$, where H and K are, respectively, the heat transfer coefficient and thermal conductivity of the cylinder, T_{amb} is the ambient temperature, and R is the cylinder radius. The solution to (2), subject to the boundary condition (3), is of the form

$$T(r,t)=T_{\mathrm{amb}}+\sum_{n=1}^{\infty}c_n J_0(\alpha_n r)\,\mathrm{e}^{-\kappa\alpha_n^2 t}, \tag{4}$$

where $J_0(.)$ is the Bessel function of order zero, and α_n is the nth root of

$$\alpha J_0'(R\alpha)+hJ_0(R\alpha)=0. \tag{5}$$

The constants c_n in (4) are mathematically determined by the initial conditions (i.e. the temperature at $t=0$). These constants and α_n are unknown in practice and are to be determined from the TOF data.

In the reconstruction problem, we use the form of (4), truncated at N terms, to approximate the unknown temperature distribution:

$$\hat{T}(r,t)=T_{\mathrm{amb}}+\sum_{n=1}^{N}c_n J_0(\alpha_n r)\,\mathrm{e}^{-\kappa\alpha_n^2 t}. \tag{6}$$

This model of the temperature contains $N+1$ undetermined parameters, namely the N coefficients, c_n, and h, which determines the constants α_n through (5). (We assume that the diffusivity, κ, and the ambient temperature, T_{amb}, are constants, and are already known.)

Now suppose, for simplicity, that the velocity–temperature relation is of the form

$$v(r,t)=v_0+\beta T(r,t), \tag{7}$$

where the constants v_0 and β are known from reference data. We note, incidentally, that the assumption of such a linear relation is not strictly necessary; that is, a more general dependence, $v=f(T)$, may be used provided only that $f(T)$ is single-valued and known over the domain of T of interest.

Now substitute (7) into (1) to give

$$\hat{\tau}(L_m,t)=\int_{L_m}\frac{\mathrm{d}l}{v_0+\beta\hat{T}(r,t)}. \tag{8}$$

The circumflexes over $\hat{\tau}$ and $\hat{T}$ indicate that the temperature model defined by (6) should be substituted for $\hat{T}$ in (8). We have also explicitly included the time dependence of the TOF measurement, $\hat{\tau}$, in (8); this is necessary if the TOF measurements are made sequentially and the temperature change between measurements is to be taken into account.

PHILOSOPHICAL TRANSACTIONS OF THE ROYAL SOCIETY A MATHEMATICAL, PHYSICAL & ENGINEERING SCIENCES

The reconstruction procedure uses an iterative algorithm to search for the $N+1$ parameters, $c_1, \ldots, c_N$ and h, that minimize the mean-square error

$$E = \sum_{m=1}^{M} [\tau(L_m, t_m) - \hat{\tau}(L_m, t_m)]^2, \tag{9}$$

where $\tau(L_m, t_m)$ is the measured TOF value along the path L_m at time t_m, and $\hat{\tau}(L_m, t_m)$ is defined by (8).

In using this approach, we note that the time origin ($t = 0$) in (6) is arbitrary, provided that the measurement times, t_m, are made relative to this origin. The resulting reconstruction will, in so far as the model (6) is good, allow the temperature to be determined at any time t relative to the time origin chosen. In our experiments, we conventionally use $t = 0$ as the time of the first TOF measurement. If, however, the TOF measurements are all performed in a period of time, Δt, such that the exponential factor, $\exp(-\kappa\alpha_n^2 \Delta t)$, does not differ significantly from one, then t_m may be set to zero for all measurements, and the exponential factor can be dropped from (6). This simplifies the nonlinear minimization of the mean-square error (9).

In many cases, the TOF measurements over different paths cannot be performed rapidly enough so that temperature drift between measurements is negligible. Under these conditions, one reasonable compromise is to substitute, in the exponential only in (6), values of α_n derived from an estimated h, obtained from cooling curves measured on similar bodies under similar thermal conditions. In this way, temperature drift can at least be approximately taken into account, while the constants α_n appearing in the argument of the Bessel function in (6) are still regarded as unknown and determined by the 'true' h by means of (5). Finally, under circumstances when knowledge of h is considered good and the thermal conditions sufficiently reproducible, this value of h can be used to determine α_n everywhere in (6). The assumption that h is known *a priori* will, of course, result in a further simplification of the mean-square-error minimization problem.

(*b*) *Rectangular symmetry reconstructions*

When the temperature distribution is bounded by a rectangle, under certain assumptions, the tomographic reconstruction problem can be greatly simplified. These assumptions may be regarded as the analogue of circular symmetry in the cylindrical temperature problem. Consider a temperature distribution on a square cross section defined by $-a \leqslant x \leqslant a$ and $-a \leqslant y \leqslant a$. (The extension to a rectangular geometry can be achieved straightforwardly.) The simplification arises if the two-dimensional temperature distribution, $T(x, y, t)$, can be factorized into the product of two one-dimensional solutions to the heat-conduction equation, i.e.:

$$T(x, y, t) - T_{\text{amb}} = f(x, t) \cdot f(y, t). \tag{10}$$

Under these conditions, the dimensionality of the problem is reduced from two to one. That is, only a single set of TOF measurements along parallel paths (i.e. one projection, say, along the x-direction of figure 3) is sufficient to recover the function $f(x, t)$, and hence $T(x, y, t)$. This contrasts with the general problem encountered, for example, in medical tomography in which hundreds of projections are required at small angular increments over 180°.

In general, it can be shown that two conditions must hold for $T(x, y, t)$ to factorize into the product of x- and y-dependent solutions (Carslaw & Jaeger 1959).

PHILOSOPHICAL TRANSACTIONS OF THE ROYAL SOCIETY A MATHEMATICAL, PHYSICAL & ENGINEERING SCIENCES

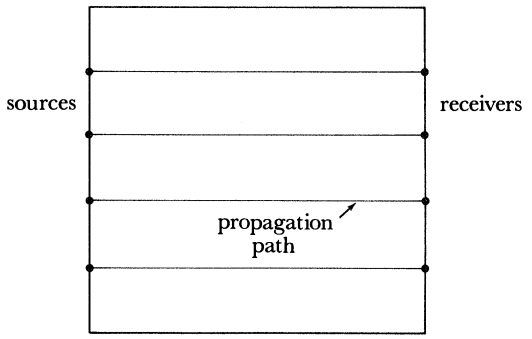

FIGURE 3. Ray paths for the reconstruction of a factorizable temperature distribution.

(i) The initial temperature distribution factors (the simplest example of this would be a uniform initial temperature):

$$T(x,y,0)-T_{\mathrm{amb}}=f(x,0)\cdot f(y,0). \tag{11}$$

(ii) The boundary conditions are spatially-uniform over each face (length $2a$) of the square boundary. That is, the boundary conditions must be expressible as:

$$\pm\partial T/\partial x+h_{\pm}(T-T_{\mathrm{amb}})=0|_{x=\pm a}, \tag{12a}$$

$$\pm\partial T/\partial y+h'_{\pm}(T-T_{\mathrm{amb}})=0|_{y=\pm a}, \tag{12b}$$

where $h_{\pm}$ signifies two values, h_{+} and h_{-}, corresponding to the boundaries $x=a$ and $x=-a$, and a similar interpretation holds for $h'_{\pm}$, corresponding to the boundaries $y=a$ and $y=-a$. In the above boundary conditions, $h_{\pm}$, $h'_{\pm}$, and T_{amb} are assumed to be constant.

Of the two conditions for factorizability just noted, the second is the more significant. This is because, provided that condition (ii) holds, even an initially unfactorizable distribution (in which (i) does not hold) will, with time, evolve rapidly toward a factorizable state. The reason for this is that the lowest-order term in the series-expansion solution to the heat-conduction equation is factorizable, and this term rapidly dominates, due to exponential damping (with time) of the higher-order terms. Stated another way, for typical values of thermal diffusivity and heat-transfer coefficient, the higher-order terms in the solution become negligible on a time scale that is a small fraction of the time required for the cylinder to cool appreciably as a whole.

Under the assumption that the two-dimensional temperature factorizes, our approach is to solve

$$\tau(y,t)=\int_{-a}^{a}\frac{\mathrm{d}x}{v(x,y,t)}, \tag{13}$$

where the velocity is of the form

$$\begin{aligned} v(x,y,t) &= v_0+\beta(T(x,y,t)-T_{\mathrm{amb}}) \\ &= v_0+\beta f(x,t)\cdot f(y,t), \end{aligned} \tag{14}$$

and v_0 and β are known constants. Thus, we have,

$$\tau(y,t)=\int_{-a}^{a}\frac{\mathrm{d}x}{v_0+\beta f(x,t)\cdot f(y,t)}, \tag{15}$$

where $\tau(y,t)$ denotes the TOF measurement performed along a path at height y and time t.

The function $f(x, t)$ can be shown to be the solution to the one-dimensional heat-conduction equation with boundary condition (12a). When the rate of heat flow out of opposite faces is the same, i.e. $h = h_+ = h_-$ and $h' = h'_+ = h'_-$, we obtain the simple result

$$f(x,t) = \sum_{n=1}^{\infty} b_n \cos(\alpha_n x)\, \mathrm{e}^{-\kappa\alpha_n^2 t}, \tag{16}$$

where α_n is the nth root of

$$\alpha \tan(\alpha a) = h. \tag{17}$$

The function $f(y, t)$ is identical in form to (16), but h is replaced by h' in (17).

As our model of temperature, we use the series (16) again truncated at N terms:

$$\hat{f}(x,t) = \sum_{n=1}^{N} b_n \cos(\alpha_n x)\, \mathrm{e}^{-\kappa\alpha_n^2 t}. \tag{18}$$

Once again, the above model is determined by $N+1$ parameters, the N coefficients b_n, and h, which determines the constants α_n through (17).

We reconstruct temperature using a least-squares approach similar to that used for the cylindrical geometry. That is, we determine the parameters that minimize

$$E = \sum_{m=1}^{M} [\tau(y_m, t_m) - \hat{\tau}(y_m, t_m)]^2, \tag{19}$$

where $\tau(y_m, t_m)$ is the measured TOF value at position y_m and time t_m, and $\hat{\tau}(y_m, t_m)$ is given by

$$\tau(y,t) = \int_{-a}^{a} \frac{\mathrm{d}x}{v_0 + \beta\hat{f}(x,t)\cdot\hat{f}(y,t)}. \tag{20}$$

in which the function $\hat{f}(.,t)$ is defined in (18).

The discussion at the end of the subsection 2a concerning the treatment of the temporal factor, $\exp(-\kappa\alpha_n^2 t)$, is relevant in this geometry as well.

The above results were derived assuming a square cross section. A similar approach can be applied to the case of a rectangular cross section for which the temperature factorizes as $T(x, y, t) - T_{\mathrm{amb}} = f(x, t)\cdot g(y, t)$. This case requires, in general, two perpendicular projections, e.g. TOF measurements over paths parallel to both the x and y axes. If, however, the heat-transfer coefficient is known on all boundaries, the rectangular cross section can be transformed by a rescaling into a square cross section, in which case the foregoing algorithm (with one projection) is again applicable.

3. Standard reference data

The theory presented above provides a basis for reconstructing a temperature distribution from TOF measurements. The accuracy of a reconstructed temperature distribution can never exceed that of the reference data that relates the ultrasonic velocity to temperature. It is essential therefore to develop reference data with an uncertainty such that errors of 5 K or less are introduced during the mapping of velocity to temperature. Because the velocity–temperature relation is sensitive to the composition (and possibly heat treatment) of the steel (Kurz & Lux 1969), it is necessary to evaluate this relation for each steel grade.

PHILOSOPHICAL TRANSACTIONS OF THE ROYAL SOCIETY A MATHEMATICAL, PHYSICAL & ENGINEERING SCIENCES

(*a*) *Experimental procedures*

To measure the temperature-dependence of velocity, we have used a modified version of the stepped bar or shoulder technique (Darbari *et al.* 1968). The sample (figure 4) consists of a cylindrical bar with a semicircular part cut from one end. This stepped end or test section is placed in the hot zone of a furnace and brought to a uniform temperature along its length. A water-cooled piezoelectric transducer is attached to the other end of the sample, and is outside the furnace. This arrangement avoids the loss of transducer sensitivity if the Curie temperature of its piezoelectric material (*ca.* 250 °C for lead zirconate titanate material used here) is approached.

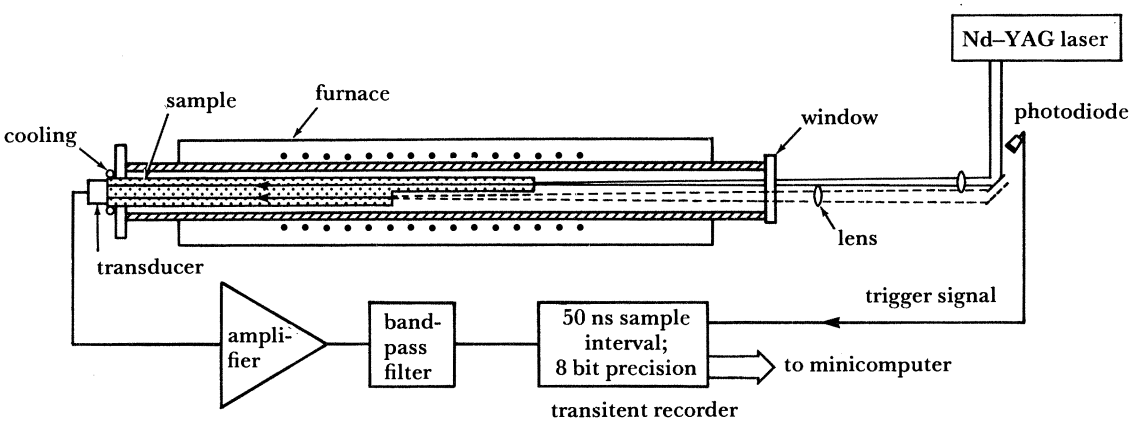

FIGURE 4. Schematic diagram of the experimental arrangement for measurement of velocity–temperature relations.

Traditionally, a pulse–echo technique is used to determine the TOFs between the transducer and step and between the transducer and test section end. Their difference is then twice the TOF in the test section. In our experiments, the echo signals were not always clearly observable owing to reflected waveguide modes returning to the transducer from the shoulder. These modes travel at velocities that are slow compared with the longitudinal waves and arrive during the time when the end echo arrives, making a TOF measurement uncertain. This problem can be eliminated by performing a transmission measurement. We have achieved this by using an intense laser pulse to generate a pair of ultrasonic pulses, alternately at the end of the sample and at the shoulder (figure 4). The TOF in the uniformly heated test section is then just the difference of the two TOF values.

The sample consists of a bar, 3.76 cm in diameter and 60 cm long, with an approximately 20 cm long test section. The length of the test section was measured to 7 μm accuracy, an uncertainty of *ca.* 1 part in 10^5. Five equispaced thermocouples were attached to the test section for accurate measurement of its temperature. The stepped part of the bar was placed in a furnace in a protective argon atmosphere, and heated at 2 K min^{-1} to a constant temperature. To overcome a small (*ca.* 20 K) temperature gradient that occurred along the test section, secondary heating coils were used to obtain a flat profile to ± 5 K.

One end of the furnace contained a window through which an infrared laser pulse could freely pass. In these experiments, a 1.09 μm wavelength pulse produced by a *Q*-switched Nd–YAG laser was used. The pulse was approximately 25 ns in duration and up to 850 mJ in energy. A lens was used to focus the pulse onto the sample.

The intense laser pulse generates an ultrasonic pulse through a combination of thermoelastic and ablation processes. This ultrasonic pulse propagated along the bar and was detected with a 2.25 MHz longitudinal transducer. The voltage signal from this transducer was amplified, filtered, and digitally recorded at a 50 ns sampling interval by using an eight-bit analogue-to-digital converter.

To determine the time-of-flight, it was necessary to indicate on the recorded trace the instant the laser pulse impinged upon the sample. This was conveniently achieved by triggering the transient recorder with the signal from a photodiode that received some of the scattered radiation of the laser pulse. The trigger pulse was also recorded at a 50 ns sampling interval.

A typical recorded waveform is shown in figure 5. Time-of-flight data could be measured to within ± 50 ns, an uncertainty of *ca.* 1 part in 10^3, sufficient for feasibility studies. Faster digitization (5 ns is now possible) and, coupled with higher-frequency transducers, could potentially improve the time-of-flight uncertainty to 1 part in 10^4, sufficiently accurate for almost all temperature-sensing problems during metals processing.

To determine the velocity from a time-of-flight measurement, accurate knowledge of the bar length at high temperature was necessary. For some steels (e.g. stainless steel), handbook values for thermal expansion coefficients are precise enough for computing acceptable corrections to the micrometer-measured ambient temperature length. For steels characterized by a body-centred cubic to face-centred cubic phase transition (ferritic steels), so much ambiguity exists in handbook thermal expansion–temperature relations that unacceptable errors are introduced. To overcome this, we developed a simple scheme for *in situ* measurement of thermal expansion for the stepped-bar samples (figure 6). The technique consisted of measuring the differential displacement between the end and the shoulder of the sample with a linear-voltage differential transformer (LVDT) attached to a pair of quartz rods of intrinsically low thermal expansion.

For all steels, the velocity of sound decreases with temperature. However, the exact relation is sensitive to the composition and possibly heat treatment of the steel (Kurz & Lux 1969). Two classes of behaviour have been observed to date, depending upon whether the ambient temperature phase was either austenite (FCC) or ferrite (BCC).

(i) *Austenitic steel data*

Figure 7 shows the temperature dependence of the longitudinal-wave ultrasonic velocity for an AISI-304 stainless steel sample between ambient temperature and 1140 °C. This steel has an FCC crystal structure throughout the range of study, and the longitudinal velocity varied monotonically with temperature. A linear fit to the data has a slope of -0.6845 ms^{-1} K^{-1} with a correlation coefficient of 0.99988. The data for both heating and cooling falls on the same line, indicating no observable sensitivity of the velocity to thermal history.

The difference between measured velocity and that interpolated from the linear fit is shown as a function of temperature in figure 8, which reveals a small sinusoidally varying error. Data points at high and low temperatures tend to lie slightly above the straight-line fit, whereas those at intermediate temperatures lie below. The origin of this variation is at present unclear. Nevertheless, correcting the linearly interpolated temperature by the curve of figure 8 could improve precision from 2 or 3 parts to *ca.* 1 part in 10^3.

PHILOSOPHICAL TRANSACTIONS OF THE ROYAL SOCIETY A MATHEMATICAL, PHYSICAL & ENGINEERING SCIENCES

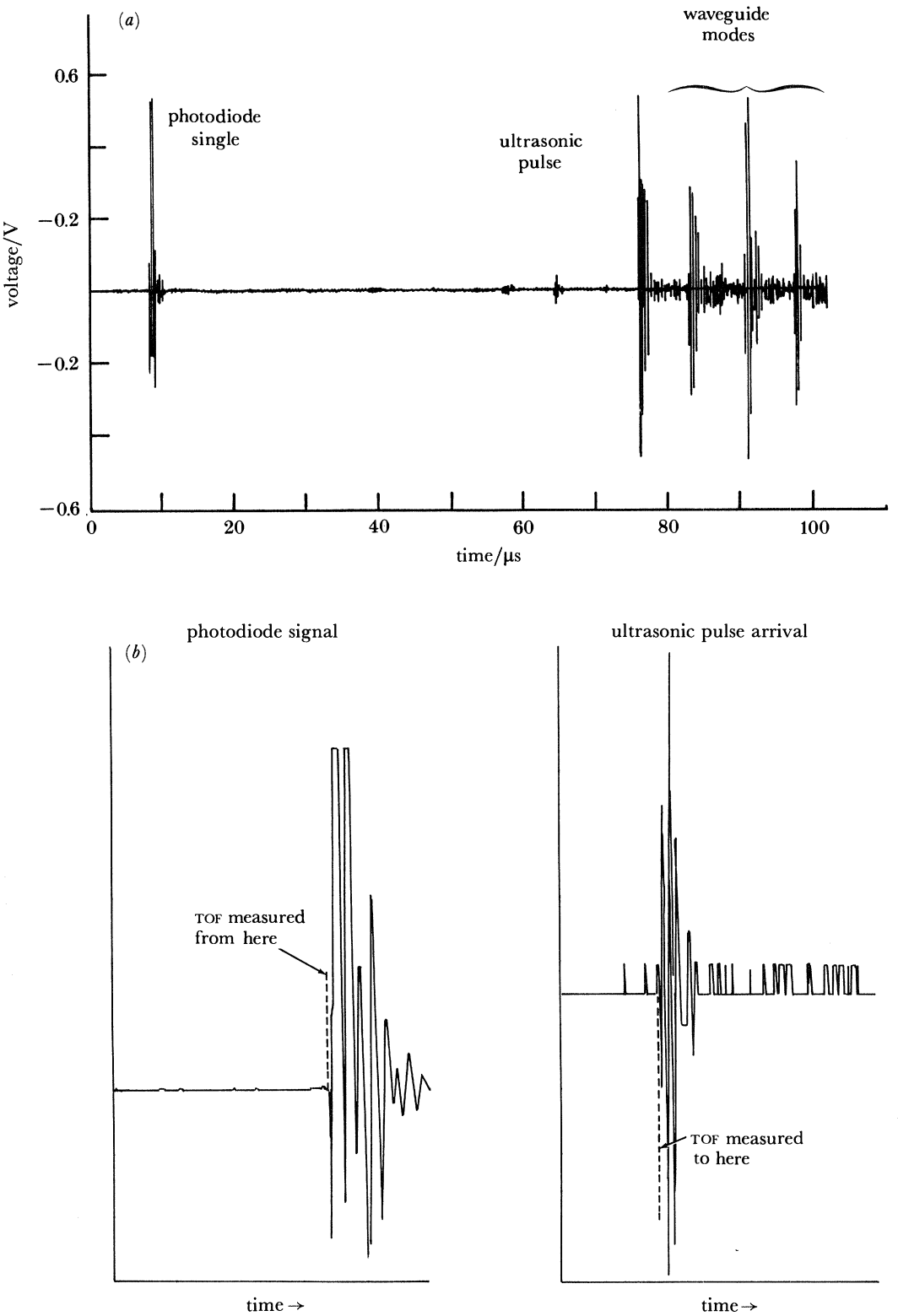

FIGURE 5. (*a*) Voltage–time waveform for laser-generated ultrasonic signal. (*b*) Expanded photodiode and longitudinal arrival signals showing where TOF was measured from.

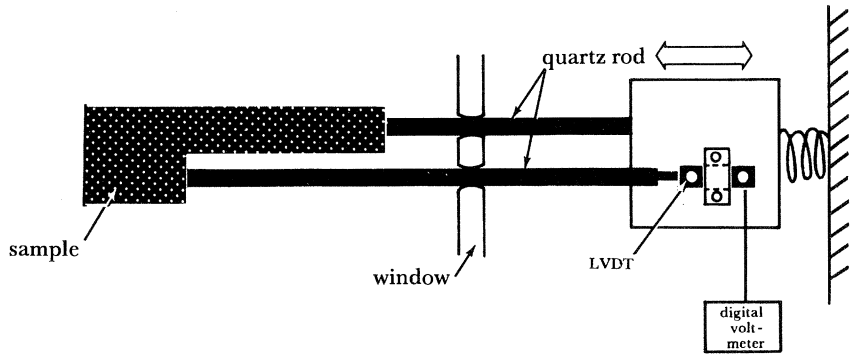

FIGURE 6. Schematic diagram of differential displacement apparatus used to correct for changes in sample length due to thermal expansion.

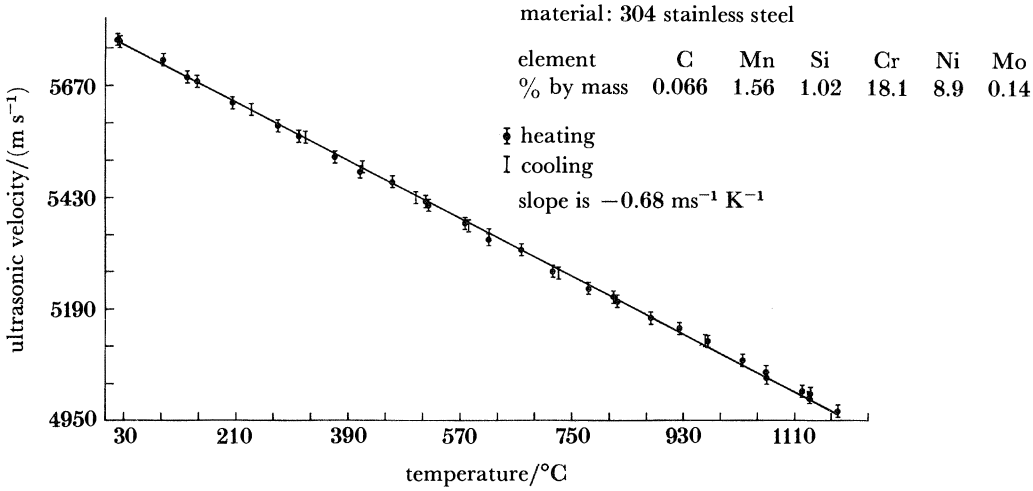

FIGURE 7. Ultrasonic velocity against temperature for AISI 304 stainless steel.

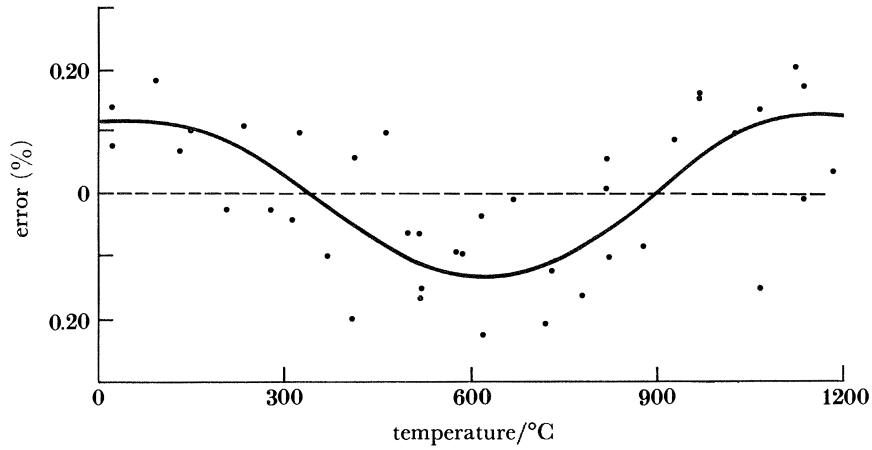

FIGURE 8. Difference (as percentage) between measured velocity and that of the linear fit as a function of temperature.

(ii) *Ferritic steel data*

The velocity–temperature data for an AISI-1018 plain-carbon steel is shown in figure 9. Whereas the velocity again decreases with temperature, the relation is more complicated than that of the austenitic steel. Three regions of behaviour are apparent.

1. Low-temperature region ($T < 730$ °C). The slope of the velocity–temperature relation increases with temperature. Heating and cooling follow the same path.

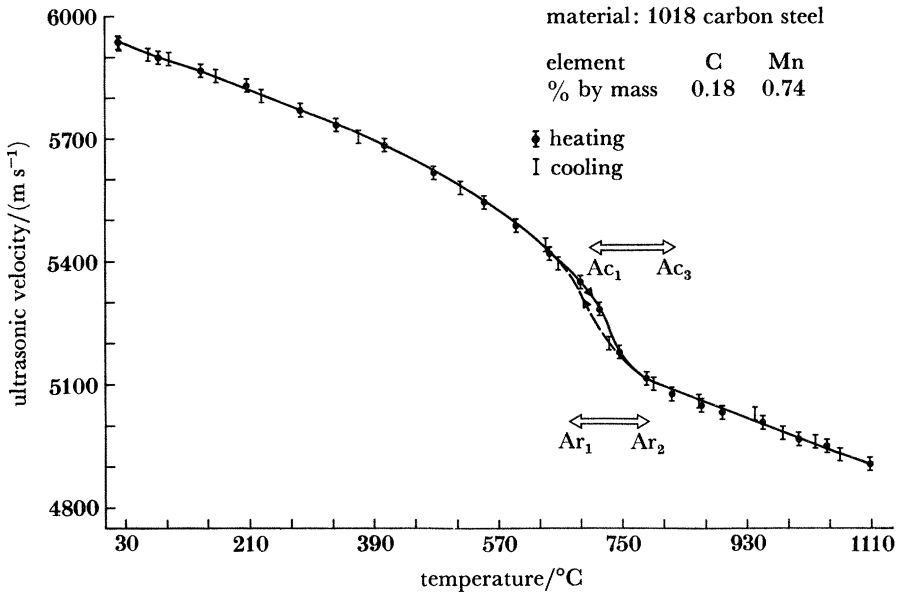

FIGURE 9. Ultrasonic velocity against temperature for AISI 1018 carbon steel.

2. Intermediate temperature region (730 °C $< T <$ 815 °C). The velocity–temperature relation goes through an inflexion point, and follows slightly different paths on heating and cooling.

3. High-temperature region ($T >$ 815 °C). The velocity–temperature relation is linear with a slope of -0.66 ms^{-1} K^{-1} and is independent of temperature path.

The origin of this added complexity is not fully understood. It could be associated with the sequence of phase changes accompanying the heating–cooling cycle and/or magnetostriction effects which disappear at the Curie temperature (768 °C for iron). A differential thermal analysis (DTA) of the steel has been performed to identify the range of temperatures over which phase transformation occurs, and this data is included in figure 9.

The phase change model proceeds as follows: the velocity of a multiphase sample can be regarded as a law of mixtures ('average') of the velocities of its microstructure constituents (α-ferrite and Fe_3C at ambient temperature). In the low-temperature region, the carbon solubility increases with temperature up to a maximum of *ca.* 0.02 % (by mass) at the eutectoid temperature Ac_1. Because the velocity in Fe_3C is greater than that of α-ferrite, an additional decrease in velocity (in addition to that of the temperature alone) would be anticipated because of carbide dissolution. This could cause a curvature of the velocity–temperature relation in the low temperature region.

At the Ac_1 temperature, determined by DTA to be 730 °C at a 2 K min^{-1} heating rate, two phenomena occur. The α-phase begins to transform to the γ-phase (FCC austenite) and Fe_3C is no longer stable and rapidly dissolves. The $\alpha \rightarrow \gamma$ transformation is complete at the Ac_3 temperature (815 °C). In this intermediate temperature region, the velocity will be an average of the velocities of the α- and γ-phases and of any metastable carbides that have not fully dissolved. The steep drop in velocity around Ac_1 may then be attributed to the rapid dissolution of carbides (their velocity being larger than either those of α or γ), as suggested by Papadakis *et al.* (1972).

Above the Ac_3 temperature, only austenite is stable (up to *ca.* 1460 °C) and no further phase or composition changes occur. The velocity is observed to follow a dependence with temperature similar to that of the austenitic stainless steel. The austenitic stainless steel contains relatively higher concentrations of Cr and Ni, and so, apparently, Cr and Ni do not have a strong influence on the slope, although they do apparently affect the ambient temperature velocity. The work of Papadakis performed with a 1 % carbon steel gave a slope in the austenite region of $-0.61\ ms^{-1}\ K^{-1}$, a possible indication that the austenite velocity slope is more sensitive to the concentration of dissolved carbon.

An alternative explanation of the velocity–temperature relation involves the magnetostriction effect. The stress field of a longitudinal wave is able to induce both a normal elastic strain (according to Hookes law) and an additional strain associated with a stress-induced magnetic domain reorientation (Mason 1958). The relative contribution of this process to the modulus (and thus ultrasonic velocity) depends upon temperature and disappears at the Curie temperature (768 °C for iron). Support for this model can be found in work on pure iron (Kurz & Lux 1969). In armco iron a similar velocity–temperature relation to the 1018 steel is observed, with a rapid velocity change around 770 °C. The magnetostriction contribution appears to be the only possible explanation of the additional complexity in pure iron since no carbides exist, and the $\alpha \rightarrow \gamma$ transformation occurs at *ca.* 910 °C, well beyond the region of the rapid velocity change. Further experiments are needed to resolve the origin of hysteresis.

In spite of this inadequate understanding of the origin of the velocity–temperature effect, the work to date indicates that, with the exception of the intermediate temperature region of ferritic steels, unique velocity–temperature relations do exist. A velocity value can be converted to temperature with sufficient accuracy for temperature-sensor needs by use of standard reference curves, especially if more accurate signal digitization is used. In practice, it is also probable that sensor needs can be satisfied even in the intermediate temperature region of ferritic steels where hysteresis occurs because heat-flow characteristics in thick materials are such that quasi-equilibrium conditions are maintained and thus hysteresis is small.

Issues that must still be addressed however are: (i) possibly steep compositional gradients in an 'as cast' ingot of steel, due to both micro and macrosegregation during solidification; (ii) broad ranges of composition within the specifications of a steel grade and (iii) textured grain structures. A detailed systematic study of these effects clearly must be performed, together with additional ultrasonic attenuation measurements to ensure that adequate high-frequency penetration is possible and unexpected composition fluctuations or textures do not introduce significant errors during the mapping of velocity to temperature.

PHILOSOPHICAL TRANSACTIONS OF THE ROYAL SOCIETY A MATHEMATICAL, PHYSICAL & ENGINEERING SCIENCES

4. Experimental temperature reconstruction

(a) *Temperature reconstructions in a cylindrical geometry*

Time-of-flight measurements were carried out on a solid cylinder of 304 stainless steel *ca.* 15.2 cm in diameter and 61 cm high by using the arrangement shown in figure 10. After being heated to approximately 700 °C in an induction heating unit, the cylinder was mounted vertically on a rotary table. An electromagnetic acoustic transducer (EMAT) was used to receive ultrasonic signals. The EMAT was mounted on the rotary table so that it rotated with the

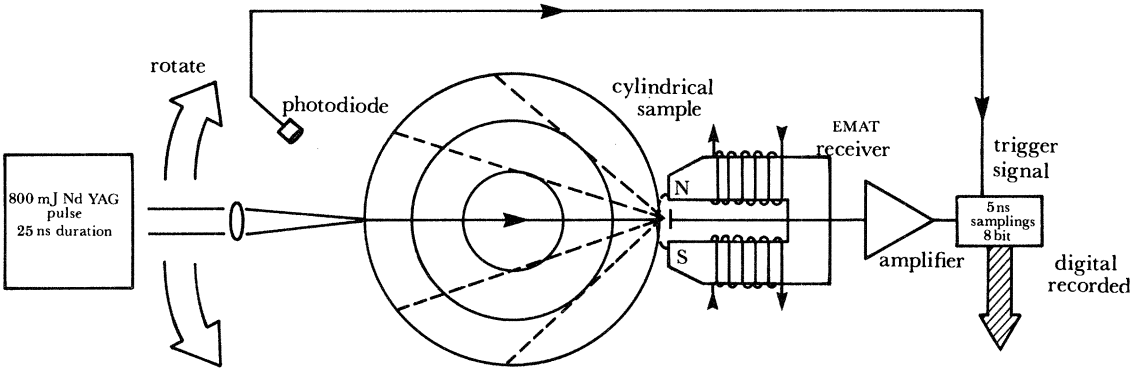

FIGURE 10. Schematic diagram of the apparatus used to measure TOF values for the cylindrical experiment.

cylinder. Its 4 mm × 4 mm sensing coil was brought to within 1 mm of the surface of the cylinder and centred on a diametrical line 25 cm above the base of the cylinder. A 850 mJ Nd–YAG laser pulse was used to generate ultrasonic pulses in an identical fashion to that described in subsection 3*a*. The incident laser beam was also made to coincide with the diametrical line at a rotary table setting of $\theta = 0°$.

By focusing the laser beam, intense ultrasonic pulses could be generated in the sample and the time-of-flight could be determined along selected chords by table rotation. The length of the rays were calculated from $L = D\cos\frac{1}{2}\theta$, where D is the diameter of the cylinder (151.968 mm at 22 °C) and θ the table rotation. Settings of 0°, ±29°, and ±50° were used. Both positive and negative θ settings were used to reduce errors resulting from eccentricity.

The received ultrasonic and trigger pulse from the photodiode were digitized (figure 11), and TOF values were derived from the digitized waveforms. Three TOF values were determined corresponding to the beginning of the first arrival, the first peak value, and a value found by fitting a straight line to the leading edge (by linear regression) and extrapolating to the baseline. Thermocouples mounted in the cylinder 38 mm above the flight path at $r = 0$, $\frac{1}{2}R$ and R, and 38 mm inches below the flight path at $r = 0$ provided a continuous record of radial and axial gradients, as well as the centre temperature. A series of measurements with the cylinder at a uniform temperature of 22 °C revealed that the computed velocities for the various paths were not constant. A correction for the width of the aperture of the EMAT coil was necessary for those paths which intersected the EMAT coil obliquely. Geometric considerations lead to a path length correction $\Delta L = \frac{1}{2}A\sin\frac{1}{2}\theta$, where A is the aperture width. This was applied to first arrival TOF velocity values using a value for $A = 4$ mm. A thermal expansion

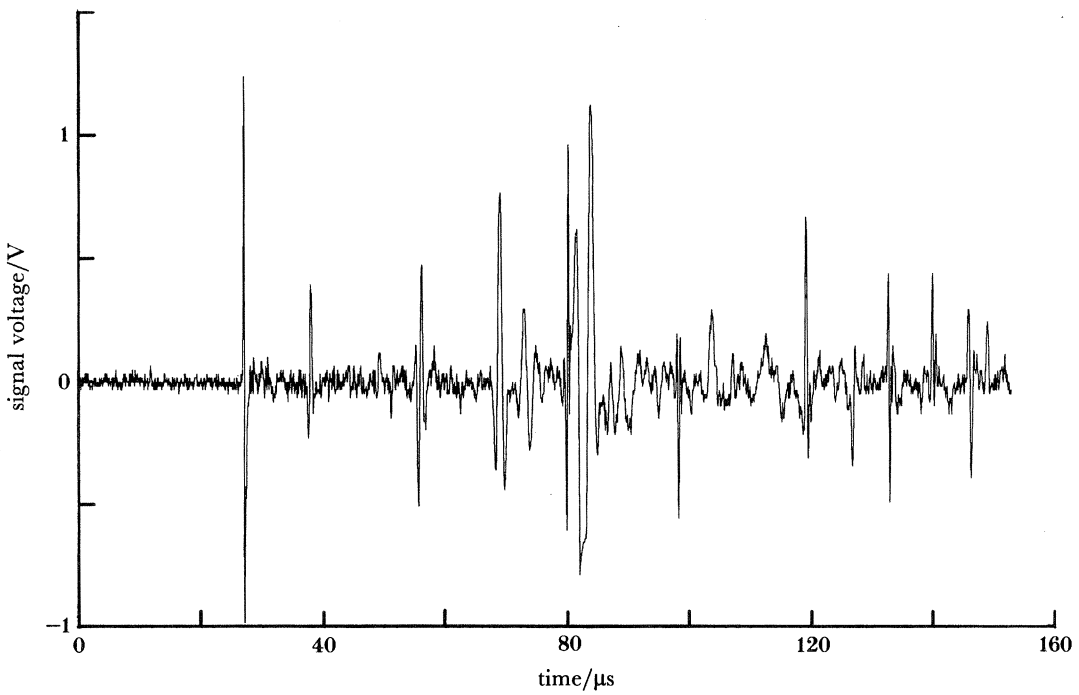

FIGURE 11. EMAT waveform for $\theta = 0°$.

correction (17×10^{-6} K^{-1}) was also applied to the path length for high-temperature velocity computations.

In our initial experiments performed on the hot cylinder, the TOF measurements were used to determine the parameters in a temperature model defined by setting $N = 1$ in (6). In this simple model, the reconstruction is determined by the two parameters c_1 of (6) and h, which determines α_1 through (5). The resulting temperature profile, which consists of the first term only of (6), should represent a good approximation to the temperature provided that terms of higher than order one have had sufficient time to damp out relative to the lowest-order term. Heat-flow simulations suggested that, for a 304 stainless steel cylinder and a uniform initial temperature, such a state is achieved in seconds.

For the above two-parameter model, we find it convenient to replace the first unknown parameter, x_1, with the new parameter T_c, where $c_1 = T_c - T_{amb}$. Thus, from (6), our temperature model may be written

$$\hat{T}(r, t) = T_{amb} + (T_c - T_{amb})\, J_0(\alpha r)\, e^{-\kappa\alpha_1^2 t}, \tag{21}$$

where α_1 is the first root of (5). Note that $T_c = \hat{T}(0, 0)$.

In figure 12*a*, we show the reconstructed temperature profile for the cylinder based upon three first arrival TOF values. An aperture correction was applied to the path lengths used for the computation of velocity. Although the reconstructed profile has approximately the correct curvature, indicating a reasonable deduced value of heat transfer coefficient, it is between 25 and 50 K below that measured with the thermocouples. This suggests that the reconstructed velocity distribution was too large, or conversely, that the TOF values were systematically too small.

PHILOSOPHICAL TRANSACTIONS OF THE ROYAL SOCIETY A MATHEMATICAL, PHYSICAL & ENGINEERING SCIENCES

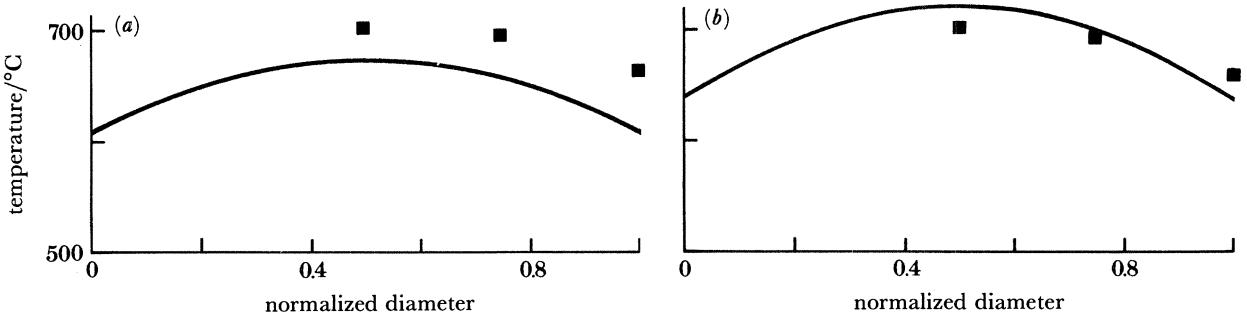

FIGURE 12. Reconstructed temperature profiles for the cylinder (curve). The square points are temperatures measured with embedded thermocouples. (*a*) Three first-arrival TOF aperture corrected measurements; (*b*) three peak TOF measurements, no aperture correction.

In figure 12*b*, we show the reconstructed profile for the same run based upon TOF values measured using the first maxima of the received waveforms ('peak' values). These were approximately 200 ns longer than the TOF values derived from the estimated first arrival. No aperture correction is necessary for the peak TOF measurements. The reconstructed temperature and the thermocouple values agree to within ± 20 K. The curvature of the distribution is similar to that of the first reconstruction, indicative of the relatively weak sensitivity of the deduced heat transfer coefficient to systematic differences in TOF.

At this point, a rule to determine the most correct TOF criterion has yet to be developed. The correct value is apparently bounded by the two shown here, and will probably depend upon the degree of high frequency attenuation experienced during pulse propagation.

(*b*) *Temperature reconstructions in a square geometry*

Time-of-flight measurements were also performed on a 304 austenitic stainless-steel block nominally 152 mm square and 37.5 cm high. The block was mounted on a translation stage so that it could be moved past the sensing coil of a stationary EMAT (figure 13). A horizontal laser beam was aligned with the EMAT coil and brought to focus at the surface of the block. The line joining the focal spot with the centre of the EMAT coil remained fixed in space as the block was translated so that measurements could be made on a series of parallel flight paths

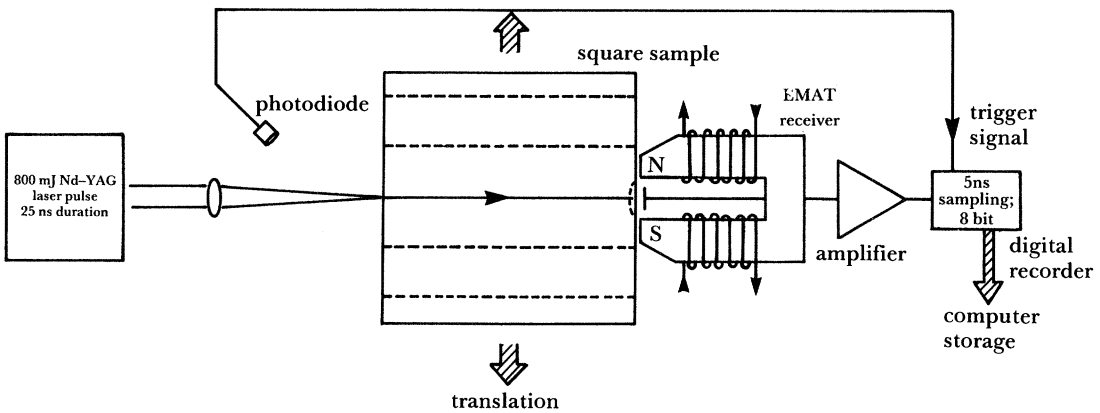

FIGURE 13. Schematic diagram of the apparatus used to measure TOF values for the square cross section experiments.

in the block at a height of 18 cm. The block could be rotated 90° to permit measurements on a second orthogonal set of paths. Five paths, 30 mm apart, were measured along each face; in each case the third path passed through the centre of the block. Five thermocouples mounted in a plane 12 mm above the plane of the flight paths were used to obtain a temperature profile for comparison with that based on ultrasonic measurements.

In our reconstruction of temperature over a square cross section, we used a temperature model defined by setting $N = 1$ in (18). In this two-parameter model, b_1 and h are determined from the TOF measurements. We also assume, for further simplicity, that the rate of heat transfer through all four faces of the steel block is the same. Then, from (18), we have

$$\hat{f}(x, t) = b_1 \cos(\alpha_1 x)\, e^{-\kappa\alpha_1^2 t}, \tag{22}$$

where α_1 is the first root of (17). For convenience, instead of using b_1 as the first unknown parameter, we again use T_c, where for this case $T_c - T_{amb} = b_1^2$. As a result, the two-dimensional temperature model becomes

$$\hat{T}(x, y, t) = T_{amb} + (T_c - T_{amb}) \cos(\alpha_1 x) \cos(\alpha_1 y)\, e^{-2\kappa\alpha_1^2 t}. \tag{23}$$

Note that $T_c = \hat{T}(0, 0, 0)$.

In figure 14, we show the reconstructed temperature distribution obtained from five TOF values for the sample at ambient temperature. Reconstructions based upon first arrival, linearly interpolated, and peak TOFs were made. The best agreement was obtained with peak arrival data at these temperatures. At much higher temperatures, the peak arrival values tended to give poorer agreement with the thermocouple data. Instead, the optimal point on the waveform for determining the TOF appeared to systematically shift nearer to the point of first arrival with increasing temperature. As noted above this effect is quite likely a result of frequency-dependent attenuation of the ultrasonic pulses, which increases with temperature.

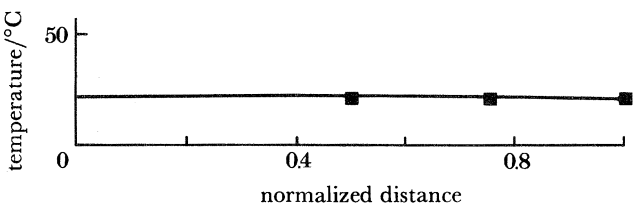

FIGURE 14. Reconstructed temperature profile for the square geometry sample at ambient temperature (5 TOF measurements). The best fit with thermocouple data was obtained with peak TOF values.

Figures 15 (*a*, *b*) show reconstructions for five time-of-flight measurements, where in one case (figure 15*a*) no correction for the temperature change between TOF measurements (*ca.* 2 min per measurement) was made, and in the second case (figure 15*b*) a cooling correction was made. The heat-transfer coefficient for this test was increased by forced air cooling. Agreement with the thermocouple data to within a few degrees is observed using peak TOF values. This improved agreement in part arises from the better conditioning of the inverse problem for this geometry.

In figure 16 (*a*, *b*), reconstructions from peak arrival TOF data are shown for two orthogonal sets of rays. Natural cooling was used and no correction for cooling between measurements was made; nevertheless, the reconstructed temperatures were within ±10 K of those measured with

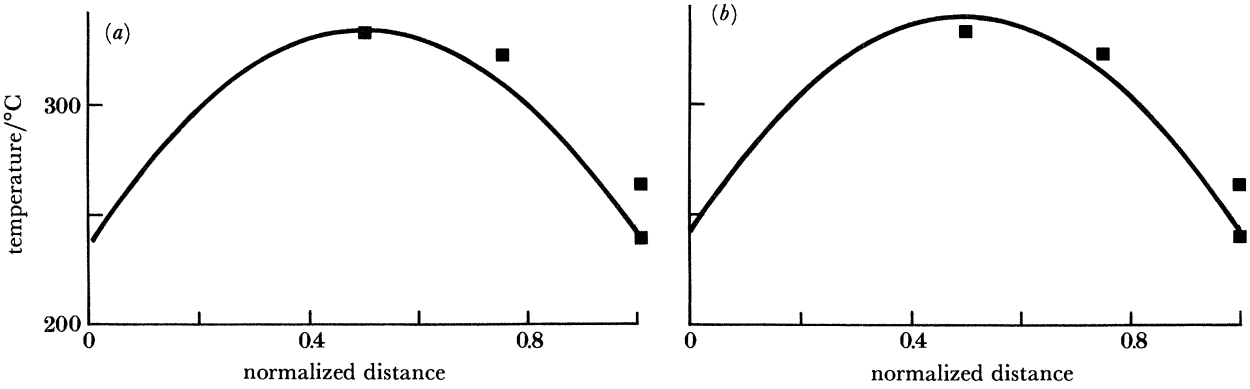

FIGURE 15. Reconstructed temperature profiles for the square geometry sample with forced air cooling in (*a*) without and in (*b*) with a temperature-drift correction.

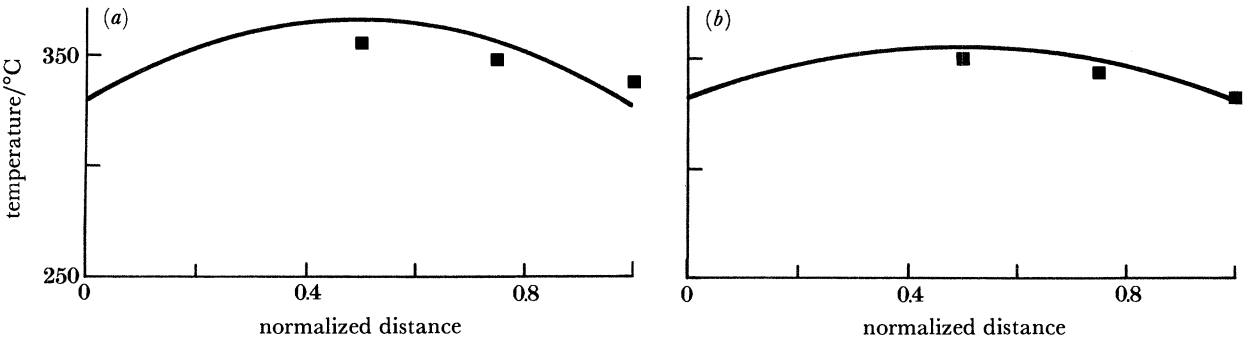

FIGURE 16. Reconstructed temperature profiles for the square geometry from two orthogonal sets of peak TOF values. (*a*) Rays 1–5 (uncorrected); (*b*) rays 6–10 (uncorrected).

thermocouples. The reconstructions showed a similar level of agreement indicative of an acceptable degree of reproducibility and justification for the heat flow approximations developed in §2*b*.

In figure 17 (*a*, *b*), reconstructions from ten first-arrival TOF measurements are shown without (*a*) and with (*b*) a correction for temperature drift between measurements. Reconstructions at these higher temperatures as discussed earlier, were invariably in better agreement with thermocouple data if first-arrival values were used.

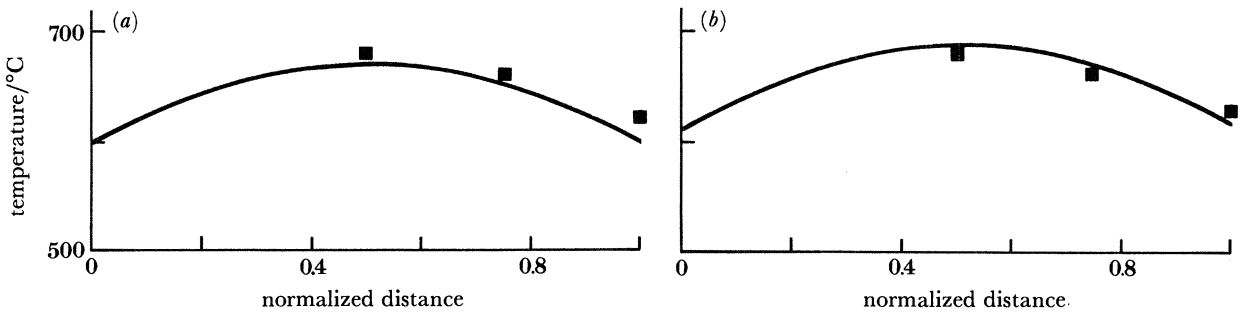

FIGURE 17. Reconstructed temperature profiles for the square geometry from both orthogonal sets of ten TOF values in (*a*) without and in (*b*) with a temperature drift correction.

An estimate was also made of the error in the TOF measurements resulting from refraction, or bending, of the ultrasonic paths. Refraction will occur whenever a component of the velocity (or temperature) gradient exists normal to the propagation path. An exact expression for the error in TOF due to refraction can be derived for the case of a constant velocity gradient normal to the line connecting the source and receiver (Norton *et al.* 1984). This expression provides a convenient worst-case estimate of the TOF refraction error and, for all experiments reported in this paper, the resulting estimated error was found to be far too small to make an observable difference in the reconstructed temperature. Further analysis suggests that only temperature gradients much larger than 100 K cm^{-1} require compensation for refraction. Such a correction could be achieved by iteration, i.e. by reconstructing temperature under the initial assumption of no refraction, and then by using ray-tracing methods to obtain an improved estimate of the true ray path, and so on. The assumption of smooth and symmetric temperature distributions will, of course, simplify the numerical task of ray tracing through the assumed distribution.

5. Summary

Non-contact techniques for TOF measurements have been used to determine internal temperature distributions in austenitic steel samples both of cylindrical and square cross section up to *ca.* 750 °C. Adequate reconstruction accuracy has been obtained for practical purposes. Discrepancies that have been discovered, may in part arise from temperature- and frequency-dependent ultrasonic attenuation that will depend upon path length. The anticipated effect of this would be to slow the rise of the broadband recorded signal used to reconstruct temperature profiles. This effect would have been unobserved in the narrowband measurements used to collect reference velocity data. Corrections for this, and thus further improved reconstructions, may be achieved by quantitative measurement of the frequency dependence of attenuation and dispersion as a function of temperature. The extension of the approach to higher temperatures then awaits only the development of higher temperature EMATS.

We express our gratitude to Dr J. Cook and Dr R. Mehrabian for their many helpful contributions to this programme and to Dr B. Maxfield who designed and constructed the EMAT. This work has been cofunded by the American Iron and Steel Institute, the NBS NDE programme office, and the Metallurgy Division of NBS.

References

Carslaw, H. S. & Jaeger, J. C. 1959 *Conduction of heat in solids*, 2nd edn. Oxford University Press.

Darbari, G. S., Sing, R. P. & Verma, G. S. 1968 *J. appl. Phys.* **39**(5), 2238–2245.

Kahn, A. H., Long, K. R., Ryckbusch, S., Hsieh, T. & Testardi, L. 1986 In *Review of progress of quantitative non-destructive evaluation* (ed. D. O. Thompson and D. E. Chimenti), vol. 5B, pp. 1383–1391. New York and London: Plenum Press.

Kurz, W. & Lux, B. 1969 *High Temp.–high Pressures* **1**, 387–399.

Mason, W. P. 1958 *Physical acoustics and the properties of solids*, pp. 209–224. Princeton, New Jersey: D. van Nostrand Company.

Mehrabian, R., Whiteley, R. L., van Reuth, E. C. & Wadley, H. N. G. 1982 Process control sensors for the steel industry. *Report of workshop, NBSIR 82-2618*. U.S. Department of Commerce.

Mehrabian, R. & Wadley, H. N. G. 1985 In *Review of progress of quantitative non-destructive evaluation* (ed. D. O. Thompson and D. E. Chimenti), vol. 4B, pp. 839–858. New York and London: Plenum Press.

Norton, S. J., Testardi, L. R. & Wadley, H. N. G. 1984 *J. Res. natn. Bur. Stand.* **89**(1), 65–74.

Papadakis, E. P., Lynnworth, L. C., Fowler, K. A. & Carnevale, E. H. 1972 *J. acoust. Soc. Am.* **52**(3), 850–857.

Discussion

E. A. Ash, F.R.S. (*Department of Electronic and Electrical Engineering, University College, London, U.K.*). One of the key problems in ultrasonic tomography is the refraction of the individually recorded beams. There is a large amount of published literature on this subject, notably in connection with breast scanners (see, for example, the publications by Professor J. Greenleaf and his group at Mayo Clinic). It would seem that the velocity gradients encountered in the metallic-rod temperature distribution problem are no less than those encountered in medical ultrasound tomography. Is this a problem? Is the existing literature on the subject applicable?

H. N. G. Wadley. Calculations have shown that the maximum velocity gradients expected under the majority of realistic conditions are much too small to make a noticeable difference in a temperature reconstruction. In fact, even under worst-case conditions, velocity gradients in hot steel are typically much less than in the human body, where abrupt changes at the boundaries between different tissue types, such as fat and muscle, may be as large as 10%. Such boundaries cause severe ray bending. Thus, I agree, refraction in medical ultrasound is certainly a problem. But, in our own experiments, refraction has not caused significant errors. For extremely large temperature gradients maintained over long propagation paths, it is true that the time-of-flight error could conceivably become large enough to warrant some correction, in which case refraction-correction techniques similar to those proposed in the medical literature, such as ray tracing, could be used here. It is worth pointing out, however, that any ray-tracing scheme, if it is necessary to use one, would be easier to apply to a temperature-induced velocity distribution, which tends to be smooth and symmetrical, than to the inhomogeneous human body, where the velocity fluctuations are more rapidly varying and random.

C. M. Sayers (*Materials Physics and Metallurgy Division, AERE Harwell, Oxfordshire, U.K.*). (*a*) In a material with a strongly varying temperature distribution, beam skewing should occur. Has Dr Wadley observed this? (*b*) I would expect that the variation of grain size and texture through the thickness of a casting would have an effect on the velocity, comparable to that of the temperature gradient. Can this be corrected for in the measurement?

H. N. G. Wadley. By beam skewing, I assume Dr Sayers means refraction. We have not observed this in our own experiments and our calculations indicate that it does not occur to any significant extent in the situations studied to date. The effects of variations in grain size and particularly of texture on velocity are, of course, much more difficult to assess and we plan to systematically investigate this phenomena in our future work. There is reason to think, however, that these effects are much smaller than the expected velocity changes due to large temperature gradients (in marked contrast to velocity changes due to residual stress). We hope that the texture and grain size effects are, at least to some extent, sufficiently random to average out when many measurements are taken over many paths.

PHILOSOPHICAL TRANSACTIONS OF THE ROYAL SOCIETY A MATHEMATICAL, PHYSICAL & ENGINEERING SCIENCES